Assessing synchronizability provided by coupling variable from the algebraic structure of dynamical systems

Christophe Letellier

Normandie Université—CORIA, Campus Universitaire du Madrillet, F-76800 Saint-Etienne du Rouvray, France

(Received 26 July 2019; revised manuscript received 16 March 2020; accepted 5 April 2020; published 29 April 2020)

Synchronization is a very generic phenomenon which can be encountered in a large variety of coupled dynamical systems. Being able to synchronize chaotic systems is strongly dependent on the nature of their coupling. Few attempts to explain such a dependency using observability and/or controllability were not fully satisfactory and synchronizability yet remained unexplained. Synchronizability can be defined as the range of coupling parameter values for which two nearly identical systems are fully synchronized. Our objective is here to investigate whether synchronizability can be related to the main rotation necessarily required for structuring any type of attractor, that is, whether synchronizability is significantly improved when the coupling variable is one of the variables involved in the main rotation. We thus propose a semianalytic procedure from a single isolated system to discard the worst variable for fully synchronizing two (nearly) identical copies of that system.

DOI: 10.1103/PhysRevE.101.042215

I. INTRODUCTION

In electronics, the phenomenon of synchronization has been investigated since at least the 1920s in coupling nearly identical valves [1], triodes [2], Audions [3–5], or feedback oscillator circuit driven by oscillations with a frequency close to the natural frequency of the former [6,7]. It was later extended to microwave oscillators [8]. Such a phenomenon became the subject of an other types of works when Pecora and Carrol considered the synchronization of two identical coupled chaotic systems [9]. Synchronization then became a topic in itself [10–13], and many applications of this phenomenon were investigated in various fields [14–17].

In Pecora and Caroll's paper, it was noted that two Lorenz systems were synchronized when they were bidirectionnally coupled by variables x or y [9]. They also obtained synchronized Rössler systems when they coupled them via variable y. The fact that the stability of the synchronous dynamics—as assessed by the master stability function [18]—was strongly dependent on the coupling variable led to the introduction of different classes of synchronization [19] as we will discuss later. When two nearly identical oscillators are coupled, there is a range in their parameter values for which the two frequencies are exactly the same (this was already defined in these terms in Ref. [4]): They are synchronized. The larger the range, the easier it is to synchronize the systems.

The easiness or the robustness to reach synchronization is strongly dependent on the nature of the coupling between the systems. In general words, such a *synchronizability* would characterize (quantify?) our ability to get a synchronous dynamics. If there are many ways to characterize the synchronization quality [11,20–22], then it is still an open question to explain why some coupling variables provide a better "synchronizability" than others. It was shown that observability, that is, assessing the possibility to distinguish different states of the original state space by using a space reconstructed from some measured variables, could contribute to explain synchronizability [23] but it was recently shown that it cannot fully explain it [24] and neither can controllability [25].

Our aim was thus to develop a way to assess the synchronizability directly from a single system (without prior numerical simulations requiring coupled systems) whose governing equations (the ordinary differential equations in the present work) are known. More specifically, we will propose a method to discard the variable not providing a robust synchronization. Since the phase is known to be one of the main ingredients for getting a good synchronization [23,26–28], it constitutes a natural "dynamical component" to consider for explaining why some variables are better than other for synchronizing dynamical systems. The idea is thus to look for the variables associated with the main rotation structuring the (chaotic) attractor which are strongly related to the phase of the dynamics. We will also investigate whether the symbolic observability coefficients as introduced in Refs. [29,30] are useful for preselecting the optimal variable for synchronizing systems. Since we showed that synchronization only weakly depends on parameter values (see Fig. 2 in the work by Letellier and Aguirre [23]), the results here obtained for a specific set of parameter values remain valid for a large domain of the parameter space.

The subsequent part of this paper is organized as follows. Section II introduces how we identify the plane associated with the main rotation. Symbolic observability coefficients and master stability functions are then briefly introduced. Five three-dimensional systems (Lorenz 63, Lorenz 84, Rössler 76, Rössler-Ortoleva, and Hindmarsh-Rose) are explicitly treated in Sec. III. In Sec. IV, the relationship between synchronizability and observability is investigated. It show also how the numerical procedure performs with respect to the analytical one. Section V provides some conclusions.

II. THEORETICAL BACKGROUND

A. The main rotation

Let us assume a dynamical system

$$\dot{\boldsymbol{x}} = \boldsymbol{f}_p(\boldsymbol{x}), \tag{1}$$

where $\boldsymbol{x} \in \mathbb{R}^m$ is the state vector and $\boldsymbol{f}_p(\boldsymbol{x})$ the vector field depending on a set of parameters $\boldsymbol{p}$. We will consider in this paper two identical systems coupled by a bidirectional dissipative linear coupling, that is,

$$\begin{aligned}
\dot{x}_1 &= f_x(\boldsymbol{x}_1) + \rho_x(x_2 - x_1)\\
\dot{y}_1 &= f_y(\boldsymbol{x}_1) + \rho_y(y_2 - y_1)\\
\dot{z}_1 &= f_z(\boldsymbol{x}_1) + \rho_z(z_2 - z_1)\\
\dot{x}_2 &= f_x(\boldsymbol{x}_2) + \rho_x(x_1 - x_2)\\
\dot{y}_2 &= f_y(\boldsymbol{x}_2) + \rho_y(y_1 - y_2)\\
\dot{z}_2 &= f_z(\boldsymbol{x}_2) + \rho_z(z_1 - z_2),
\end{aligned} \tag{2}$$

where a single coupling coefficient ρ_c $(c \in \{x, y, z\})$ is nonzero. Our objective is to discard the variable providing the most difficult full synchronization.

In most of the cases, an attractor is structured, in the state space, around singular points of the saddle-focus type, the focus being unstable. When there is no singular point, it was shown that a singularity was present, with a transverse stability associated with an unstable singular point [31]. Chaotic attractors are always structured by a spiralling structure combined with a switch mechanism, even when there is no singular point [32]. An obvious example is provided by homoclinic chaos [33–35]. In this case, there is clearly a two-dimensional (unstable or stable) manifold associated with a spiralling structure. This would correspond to a pair of singular points with complex conjugated eigenvalues with positive real parts. In that case, the spiral diverges from the singular point but there are few exceptions as the cord attractor [36].

Since the phase is a key characteristics for assessing the type of synchronization, our objective is to investigate whether the osculating plane of the spiral structuring the attractor coud be useful to discriminate various qualities of synchronizability offered by the variables of the system. By definition, the two variables spanning this plane must have the information about the phase of the dynamics, an information which is required for a full synchronization [23,26–28,37]. These two variables should be then preferred for coupling the systems to synchronize. When two rotations are involved for structuring the attractor, as observed in the Rössler system when the dynamics is non phase-coherent [38], there is one primary rotation acting during most—if not all—of the revolution in the attractor while the secondary one (associated with the reinjection mechanism required for producing chaotic dynamics [32]) is only active during a fraction of this revolution (this will be more detailed in Sec. III A with the Rössler system).

For three-dimensional systems, it is therefore required to choose among the three possible planes (x-y, x-z, or y-z) the one that is the most parallel to the osculating plane of the primary rotation. We would like to do this by analytical computations, directly from the algebraic structure of the governing equations. When the algebraic complexity of the system becomes too large for these computations, we will propose a numerical evaluation.

Let us start with the analytical approach for identifying the variables spanning the main rotation. It is based on the set of 1-regular points introduced for describing the structure of systems without any singular point [31]. For m-dimensional dynamical systems, the 1-regular points are defined by vanishing $m-1$ derivatives. Let designate by $\mathcal{S}_i$ the set of 1-regular points for which only the ith derivative is nonzero. Along set $\mathcal{S}_i$, a stability analysis based on the Jacobian matrix is performed in the plane defined by the null derivatives to determine the "transverse" stability. Rotation and torsion are associated with a set of complex conjugated eigenvalues. The main torsion will be associated with the set $\mathcal{S}_i$ whose most of it has a transverse stability characterized by complex eigenvalues.

When the algebraic structure of the system is too complicated (high-dimensional, high-order nonlinearity or rational terms), this analytical approach quickly leads to inextricable computations. In this case, we propose to use a simple numerical technique to determine the main plane of rotation and thus to discard the variable not providing a good synchronizability. A possible way to characterize a spiral (roughly a circular motion with a drifting radius) is to consider that the distance between the trajectory and the singular point surrounded by the attractor is more or less constant. Let be

$$r(t) = \sqrt{(u_j - u_j^*)^2 + (u_k - u_k^*)^2} \tag{3}$$

the radius of the spiral evaluated in the two-dimensional plane u_j-u_k where the singular point surrounded by the attractor has coordinates u_j^* and u_k^*. We assumed that when the plane u_j-u_k is the best approximation of the rotation plane, the corresponding mean derivative $\bar{r}$ is the smallest. The numerical derivative $\dot{r}$ is computed at each time step (using a Euler scheme) and averaged along a trajectory made of at least 20 revolutions. It thus allows to select the plane associated with the main rotation.

B. Symbolic observability coefficients

Since it was previously attempted to make a link between synchronizability and observability [23], we will investigate whether these two concepts are actually related. In order to do that, we will use the symbolic observability coefficients η_i. Observability is related to the possibility to distinguish different states in the original state space by only measuring some of its variables [39]. In short, the coordinate transformation Φ_s between the original state space $\mathbb{R}^3(\boldsymbol{x})$ and the "reconstructed" space $\mathbb{R}^3(\boldsymbol{X})$ spanned by the "measured" variable s and its first two derivatives provides a full observability of $\mathbb{R}^3(\boldsymbol{x})$ when

$$\mathrm{Det}\, \mathcal{J}_{\Phi_s}(\boldsymbol{x}) \neq 0 \quad (\forall \boldsymbol{x} \in \mathbb{R}^3) \tag{4}$$

(see Refs. [39,40] for more details). The "yes-or-no" answer provided by such a criterion was extended by introducting observability coefficients [41] which can be computed using a symbolic approach (see Refs. [29,30] for more details). These observability coefficients can be viewed as the probability that the trajectory representative of the system evolution is out of the neighborhood of the singular observability

manifold defined by $\mathrm{Det}\mathcal{J}_{\Phi_s}(\boldsymbol{x}) = 0$ [42]. When the symbolic observability coefficient $\eta_s = 1$, there is a full observability (the determinant $\mathrm{Det}\mathcal{J}_{\Phi_s}(\boldsymbol{x})$ never vanishes). Contrary to this, when $\eta_s = 0$, no state of the original state space can be observed. Typically, a good observability is provided when $\eta_s > 0.75$ [24].

C. Master stability functions

In order to investigate the synchronizability of dynamical systems, Pecora and Caroll introduced the concept of master stability function (MSF) [18] which gives a necessary (but not sufficient) condition under which a specific coupling (network) configuration leads to a synchronous evolution for a particular (local) oscillator dynamics. Typically, two identical systems $\dot{\boldsymbol{x}} = \boldsymbol{f}(\boldsymbol{x})$ can be synchronized when the largest Lyapunov exponent Λ_s characterizing the variational equation

$$\dot{\boldsymbol{\zeta}} = [\mathcal{J}_f(\boldsymbol{x}^s) - \mu\mathcal{J}_h(\boldsymbol{x}^s)]\boldsymbol{\zeta} \tag{5}$$

is negative. In Eq. (5), $\boldsymbol{\zeta}$ are the eigenvectors of the coupling matrix, $\mathcal{J}_f$ is the Jacobian matrix of the system considered, $\mathcal{J}_h$ is the Jacobian matrix of the measurement function h, and μ is the normalized coupling parameter [18]. which is related to ρ_s according to $\rho_s = \frac{\mu}{2}$ when two system are coupled. From the number of zeros of the master stability functions, three classes of synchronization were introduced [19]. As discussed in Ref. [24], these classes can be defined as follows:

(i) Class I (one zero) corresponds to a MSF remaining negative for any $\mu > \mu_m$, meaning that the networked systems can be synchronized for any coupling strength greater than a threshold value μ_m;

(ii) Class II (two zeros) corresponds to a MSF being negative within a range $\mu \in [\mu_m; \mu_M]$, meaning that there is a finite interval for the coupling strength for which the networked systems can be synchronized;

(iii) Class III (no zero) corresponds to a MSF remaining positive for any μ value, meaning that the networked systems can never be synchronized for any coupling strength.

The three classes are thus numbered from the easiest configuration for getting synchronzation (class I) to the most difficult one (class III).

III. RESULTS

Five three-dimensional systems whose dynamics are very different were used for testing our procedure for discarding the worst coupling variable to fully synchronize dynamical systems. We only reported the analysis of the set of 1-regular points which can be associated with rotation.

A. The Rössler system

The Rössler 76 system [43],

$$\begin{aligned}\dot{x} &= -y - z\\ \dot{y} &= x + ay\\ \dot{z} &= b + z(x - c),\end{aligned} \tag{6}$$

produces a chaotic attractor characterized by a one-dimensional three-modal map for $a = 0.520$, $b = 2$, and $c = 4$ (Fig. 1). It is structured around two singular points

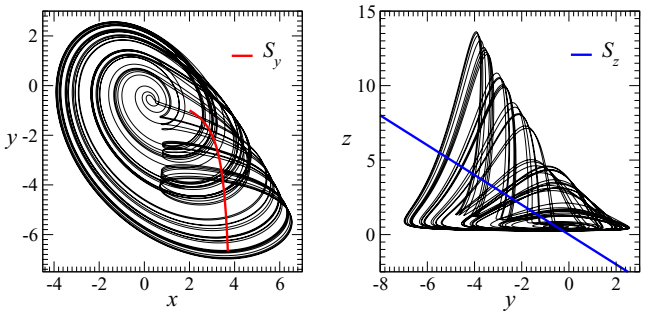

FIG. 1. Three-modal chaotic attractor produced by the Rössler system. The sets $\mathcal{S}_y$ (red) and $\mathcal{S}_z$ (blue) are also plotted in the x-y and y-z planes, respectively. Parameter values: $a = 0.520$, $b = 2$, and $c = 4$.

$$S_\pm = \begin{vmatrix} x_\pm = az_\pm \\ y_\pm = -z_\pm \\ z_\pm = \frac{c \pm \sqrt{c^2 - 4ab}}{2a} \end{vmatrix}. \tag{7}$$

S_- is the point at the center of the divergent spiral associated with the main rotation of the attractor: its eigenvalues are

$$\lambda_- = \begin{vmatrix} 0.190 \pm 0.962i \\ -3.580\,. \end{vmatrix} \tag{8}$$

The second singular point S_+ is not surrounded by the attractor and is characterized by the pair of complex conjugated eigenvalues

$$\lambda_+ = \begin{vmatrix} -0.092 \pm 2.842i \\ 0.425 \end{vmatrix}. \tag{9}$$

It is active during the nonlinear switch [38].

The set $\mathcal{S}_x$—defined by $\dot{y} = \dot{z} = 0$ and $\dot{x} \neq 0$—is associated with the eigenvalues $\lambda_1 = a$ and $\lambda_2 = x - c$. The y-z plane cannot therefore be associated with the main rotation. The set

$$\mathcal{S}_y = \begin{vmatrix} x = c + \frac{b}{y} \\ z = -y \end{vmatrix} \tag{10}$$

is associated with the eigenvalues

$$\lambda_\pm = \frac{b + \sqrt{b^2 + 4y^3}}{y}, \tag{11}$$

which are complex conjugated when $y^3 < \frac{b^2}{4}$, that is, when $y < -1$ for $b = 2$. This spiralling structure of the flow is clearly associated with the auxiliary rotation responsible for the nonlinear switch. The set

$$\mathcal{S}_z = \begin{vmatrix} x = a \\ z = -y \end{vmatrix} \tag{12}$$

is associated with the eigenvalues

$$\lambda_\pm = \frac{a + \sqrt{a^2 - 4}}{2} \tag{13}$$

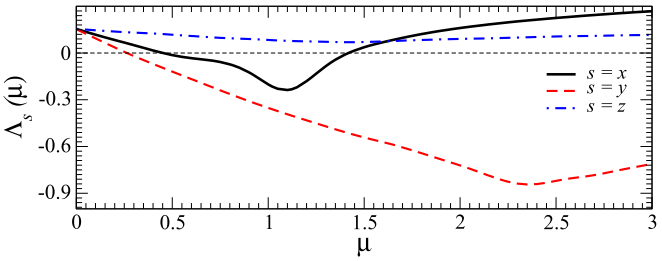

FIG. 2. Master stability functions $\Lambda_s(\mu)$ versus the normalized coupling parameter μ computed for Rössler 76 systems successively coupled via each of their three variables. Same parameter values as in Fig. 1.

which are complex conjugated when $|a| < 2$, a condition always holding when there is a chaotic attractor ($a \in [0.386; 0.556]$ with $b = 2$ and $c = 4$ as detailed in Ref. [38]). The x-y plane is nearly parallel to the main spiralling structure of the flow, that is, to the two-dimensional unstable manifold of the saddle-focus point around which is structured this attractor [38]. Variable z should therefore be discarded for synchronizing Rössler systems since it does not contain information on the phase of the main rotation.

The master stability functions (Fig. 2) are such as variable y provides a class I synchronization, variable x a class II synchronization and variable z a class III synchronization. Our analysis thus correctly rejected the worst variable for synchronizing Rössler systems.

B. The Lorenz 84 system

In 1984 Edward Lorenz proposed a simple model for the global atmospheric circulation [44]. It is governed by the set of three differential equations

$$\begin{aligned} \dot{x} &= -y^2 - z^2 - ax + aF \\ \dot{y} &= xy - bxz - y + G \\ \dot{z} &= bxy + xz - z \end{aligned} \tag{14}$$

producing the chaotic attractor (Fig. 3) with a toroïdal structure. This system is weakly dissipative [45]. This attractor is structured around a single singular point S whose coordinates are $x = 8$, $y = -0.007$, and $z = 0.03$. This is a saddle-focus

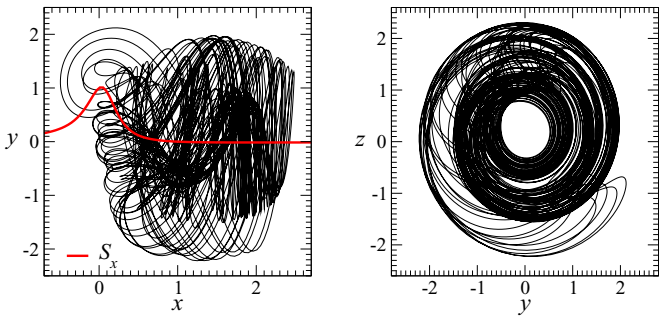

FIG. 3. Chaotic attractor produced by the Lorenz 84 system (14). The set $\mathcal{S}_x$ is plotted as a thick red curve in the x-y plane. The y-z plane projection evidences the main rotation driving the dynamics. Parameter values: $a = 0.28$, $b = 4$, $F = 8$, and $G = 1$.

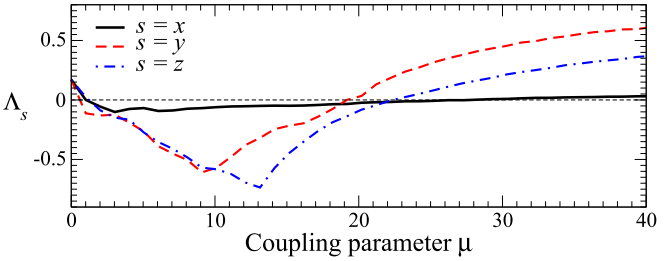

FIG. 4. Master stability functions for identical Lorenz 84 system successively coupled by each of their three variables. Same parameter values as in Fig. 3.

point characterized by the eigenvalues

$$\lambda = \begin{vmatrix} 7.00 \pm 31.99\, i \\ -0.280 \end{vmatrix}. \tag{15}$$

The singular set

$$\mathcal{S}_x = \begin{vmatrix} y = -\frac{G(x-1)}{(x-1)^2 + b^2x^2} \\ z = -\frac{bGx}{(x-1)^2 + b^2x^2} \end{vmatrix} \tag{16}$$

is always defined since $(x-1)^2 + b^2x^2$ never vanishes. The corresponding eigenvalues $\lambda_\pm = x - 1 \pm i\, bx$ are complex conjugated until $x \neq 0$. This means that the flow is always rotating in the y-z plane with the exception of the plane defined by $x = 0$ which corresponds to the plane where the rotation is inverted (clockwise for $x < 0$ and anticlockwise for $x > 0$). The main rotation is therefore associated with the y-z plane and variable x has no information about its phase. It should be avoided for synchronizing Lorenz 84 systems. Due to the large number ($n = 6$) of nonlinear terms, the Lorenz 84 system has singular sets $\mathcal{S}_y$ and $\mathcal{S}_z$, which are too complicated to be easily investigated here.

According to the master stability functions (Fig. 4), all variables provide class II synchronization. Nevertheless, the more negative the master stability function, the easier the synchronization. In the case of a coupling via variable x, the master stability function is only slightly negative compared to the two other ones. Lorenz 84 systems do not present robust synchronization against noise contamination or differences between the two systems. Contrary to this, when $\rho_y \in [2.1; 7.9]$ and $\rho_z \in [2.1; 8.9]$, the master stability function is strongly negative (class II synchronization) and a full synchronization is easily obtained in both cases. These master stability functions thus confirm our rejection of variable x for synchronizing Lorenz 84 systems.

C. The Lorenz 63 system

We now consider the Lorenz 63 system [46]

$$\begin{aligned} \dot{x} &= \sigma(y - x) \\ \dot{y} &= Rx - y - xz \\ \dot{z} &= -bz + xy, \end{aligned} \tag{17}$$

which is equivariant under a $\mathcal{R}_z$ rotation symmetry around the z axis [47]. This global property of the system is crucial to consider for synchronization because symmetries are known

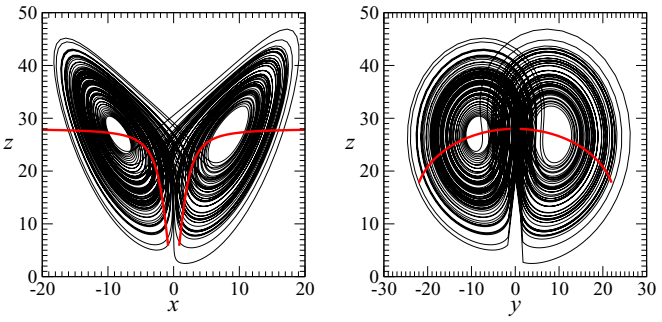

FIG. 5. Chaotic attractor produced by the Lorenz 63 system (17). The singular set $\mathcal{S}_x$ is plotted as a thick red line in the two plane projections. Parameter values: $\sigma = 10$, $b = 8/3$, and $R = 28$.

to be responsible for a lack of synchronization [23]. Indeed, variable z is left invariant under the rotation symmetry and cannot allow a full synchronization, mainly because it has no information about the wing which is visited.

The Lorenz attractor is structured around three singular points, the origin of the state space S_0 and two symmetry-related singular points,

$$S_\pm = \begin{vmatrix} \pm\sqrt{b(R-1)} \\ \pm\sqrt{b(R-1)}, \\ R-1 \end{vmatrix} \tag{18}$$

which are saddle-focus points associated with eigenvalues

$$\lambda_\pm = \begin{vmatrix} 0.094 \pm 10.19i \\ -13.85 \end{vmatrix} \tag{19}$$

for the parameter values $R = 28$, $\sigma = 10$, and $b = \frac{8}{3}$. In this case, the so-called Lorenz attractor is obtained (Fig. 5). These two saddle-focus points are the two points surrounded by the flow.

The singular set

$$\mathcal{S}_x \equiv \begin{vmatrix} y = \frac{bRx}{b+x^2} \\ z = \frac{xy}{b} \end{vmatrix} \tag{20}$$

is associated with the eigenvalues

$$\lambda_\pm = \frac{-(b+1) \pm \sqrt{(b-1)^2 - 4x^2}}{2}, \tag{21}$$

which are complex conjugated when $|x| > \frac{b-1}{2}$, that is, for $|x| > 1.154$. Most of the attractor is therefore associated with a spiralling structure in the y-z plane. The domain for which there is no rotation corresponds to the switch from one wing to the other. When the trajectory remains in a given wing, it is mainly driven by this rotation. The singular set $\mathcal{S}_y$ and $\mathcal{S}_z$ are associated with real eigenvalues and cannot induce a spiralling structure.

The set $\mathcal{S}_x$ is associated with the main rotation and variable x must be therefore avoided for synchronizing Lorenz 63 systems. Variable z can be discarded with symmetry arguments. Variable y is thus the best one for synchronizing Lorenz 63 systems. The master stability functions for identical Lorenz 63 systems are shown in Fig. 6. Variable z is the worst coupling

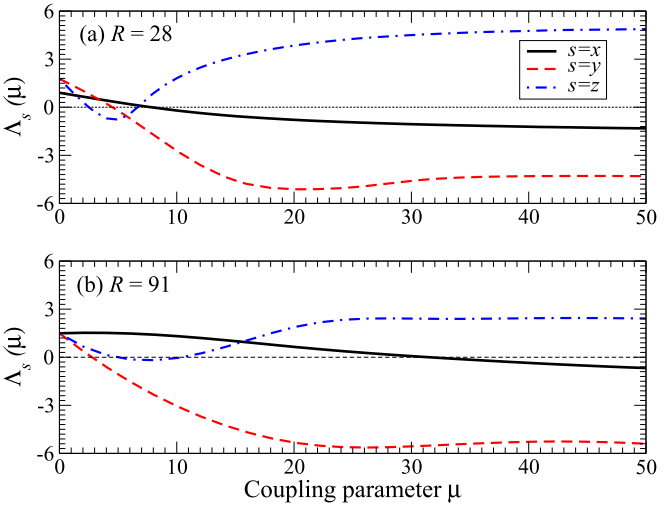

FIG. 6. Master stability functions $\Lambda_s(\mu)$ versus the normalized coupling parameter μ computed for Lorenz systems successively coupled via each of their three variables.

variable (class II synchronization with a very small negativity) for synchronizing Lorenz 63 systems. Variable x provides a class I synchronization but with a small negativity: The synchronization is therefore not robust. If it is actually possible to synchronize through variable x two identical Lorenz systems, this is not the case when there is a parameter mismatch as shown in Fig. 7. This result shows that variable x does not provide a robust synchronization and is clearly not a recommendable choice.

This confirms our rejection of variable x for coupling Lorenz 63 systems since it does not have information about the main rotation of the flow. In addition to that, variable z is rejected for symmetry reasons. Variable y is associated with a class I synchronization with a strongly negative master stability function.

D. The Hindmarsh-Rose system

Another atypical system is the Hindmarsh-Rose system. Originated from the Hodgkin-Huxley model [48] that Richard

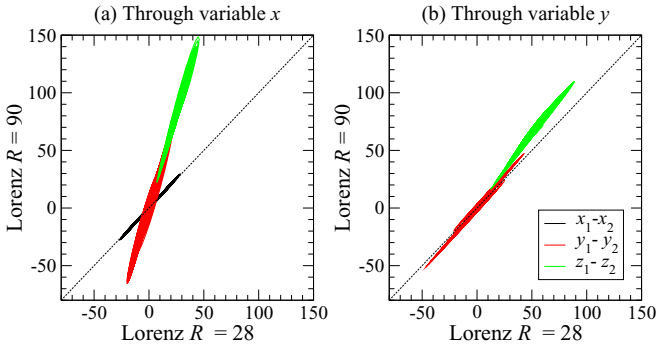

FIG. 7. Two different Lorenz systems coupled through variable x (a) and y (b). $R_1 = 28$ and $R_2 = 91$, $\sigma = 10$, and $b = \frac{8}{3}$. The synchronization is partial (only the coupled variables are fully synchronized, the two others do not fluctuate within the same range) in case (a) while there is a full synchronization in case (b).

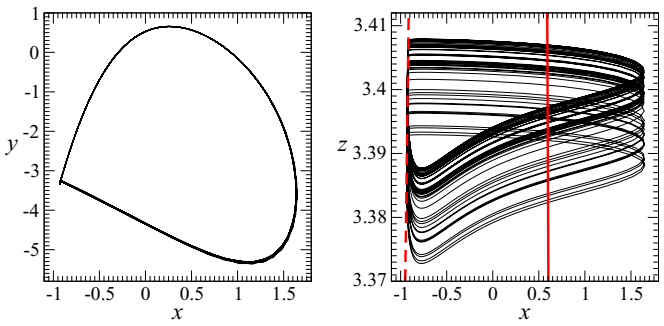

FIG. 8. Chaotic attractor produced by the Hindmarsh-Rose system (22). The singular set $\mathcal{S}_z$ is plotted in a solid red line when it has complex conjugated eigenvalues and in a dashed red line otherwise. Parameter values: $a = 3$, $b = 3$, $c = 1$, $d = 5$, $s = 4$, $X_c = -\frac{1+\sqrt{5}}{2}$, $r = 0.001$, and $I = 3.318$.

FitzHugh replaces with a second-order differential equation [49], Hindmarsh and Rose added a third equation to limit the neuron firing [50]. The resulting model is

$$\begin{aligned}\dot{x} &= I + y - z + bx^2 - ax^3\\ \dot{y} &= c - y - dx^2\\ \dot{z} &= r[s(x - X_c) - z],\end{aligned} \tag{22}$$

where x is the membrane potential, y the recovery variable (quantifying the transport of sodium and potassium through fast ion channels), and z an adaptation current which gradually hyperpolarizes the cell (it corresponds to the transport of other ions through slow channels). A chaotic attractor can be (Fig. 8) produced by system (22). With the parameter values used in Fig. 8, there is a single singular point

$$S = \begin{vmatrix}-0.563\\ -0.586,\\ 4.219\end{vmatrix} \tag{23}$$

which is characterized by real eigenvalues. It is neither surrounded by the attractor nor associated with complex conjugated eigenvalues. It is therefore not associated with the main rotation.

The set $\mathcal{S}_x$ is associated with real eigenvalues. The second singular set,

$$\mathcal{S}_y = \begin{vmatrix}y = ax^3 - bx^2 + s(x - X_c) - I\\ z = s(x - X_c)\end{vmatrix}, \tag{24}$$

is associated with the eigenvalues

$$\lambda_y = \frac{2bx - 3ax^2 - r \pm \sqrt{(2bx - 3ax^2 + r)^2 - 4rs}}{2}, \tag{25}$$

which are complex conjugated when $|x| < 0.021$ with the parameter values used in Fig. 8, that is, far from the attractor [since $z > 6$ according to Eq. (24)]: It cannot be responsible for the main rotation. The last singular set,

$$\mathcal{S}_z = \begin{vmatrix}y = c - dx^2\\ z = -ax^3 + (b - d)x^2 + c + I\end{vmatrix}, \tag{26}$$

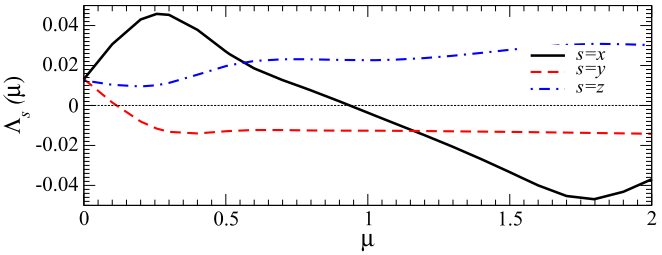

FIG. 9. Master stability functions $\Lambda_s(\mu)$ versus the normalized coupling parameter μ for the Hindmarsh-Rose systems successively coupled via each of their three variables. Parameter values as in Fig. 8.

is associated with the eigenvalues

$$\lambda_z = \frac{2bx - 3ax^2 - 1 \pm \sqrt{(2bx - 3ax^2 + 1)^2 - 8dx}}{2}, \tag{27}$$

which are complex conjugated when $0.036 < x < 1.353$, that is, during most of the main oscillation (left panel in Fig. 8). This singular set is therefore responsible for the main rotation which is thus parallel to the x-y plane. Variable z can be therefore discarded for synchronizing Hindmarsh-Rose systems as confirmed by the master stability functions (Fig. 9) since Λ_z is always positive.

E. The Rössler-Ortoleva system

With Peter Ortoleva, Rössler proposed the system [51]

$$\begin{aligned}\dot{x} &= ax + by - cxy - \frac{(dz + e)x}{x + K_1}\\ \dot{y} &= f + gz - hy - \frac{jxy}{y + K_2}\\ \dot{z} &= k + lxz - mz,\end{aligned} \tag{28}$$

producing a chaotic attractor [Fig. 10(a)] which has a very different topological structure than the previous ones. It is characterized by a unimodal map with a cusp at its maximum

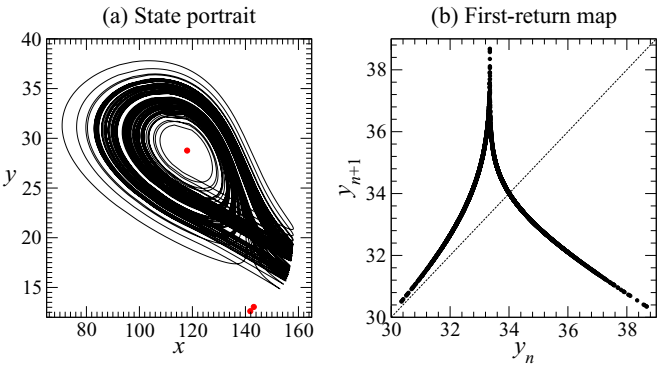

FIG. 10. Unimodal torn chaotic attractor produced by the Rössler-Ortoleva system (28). The three singular points in the neighborhood of the attractor are also shown (red points). Parameter values: $a = 33$, $b = 150$, $c = 1$, $d = 3.5$, $e = 4815$, $f = 410$, $g = 0.59$, $h = 4$, $j = 2.5$, $k = 2.5$, $l = 5.29$, $m = 750$, $K_1 = 0.010$, and $K_2 = 0.010$.

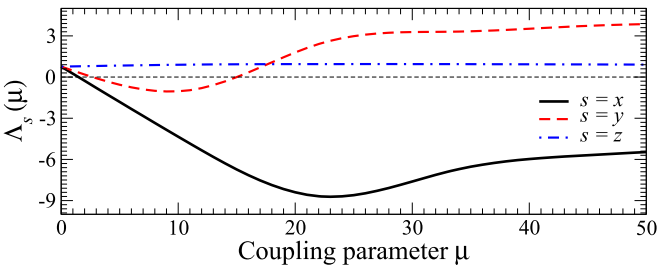

FIG. 11. Master stability functions $\Lambda_s(\mu)$ versus the normalized coupling parameter μ computed for Rössler-Ortoleva systems successively coupled *via* each of their three variables. Parameter values as in Fig. 10.

[Fig. 10(b)]. This is a characteristic signature of an attractor with a tearing mechanism (and not a folding, as observed in the Rössler attractor) [52]. For the parameter values used in Fig. 10, there are seven singular points, but only three of them are in the neighborhood of the attractor. They are

$$S_1 = \begin{vmatrix} 141.83 \\ 12.61 \\ -8.93 \end{vmatrix}, \quad S_2 = \begin{vmatrix} 143.16 \\ 13.04 \\ -0.34 \end{vmatrix}, \quad \text{and } S_3 = \begin{vmatrix} 118.02 \\ 28.77 \\ 0.02 \end{vmatrix}. \quad (29)$$

Their corresponding eigenvalues are

$$\lambda_1 = \begin{vmatrix} 25.9 \\ -2.4, \\ -6.9 \end{vmatrix}, \quad \lambda_2 = \begin{vmatrix} 19.7 \\ 6.8 \\ -3.3 \end{vmatrix}, \quad \text{and } \lambda_3 = \begin{vmatrix} 0.1 \pm 7.9i \\ -125.7 \end{vmatrix}, \quad (30)$$

respectively. Point S_3 is the single one being surrounded by the flow: It is a saddle-focus point.

The two rational terms in the first two equations of system (28) prevent a successful analysis of the singular sets of 1-regular points, the equations being too complicated to be handled. We therefore need to use the numerical approach based on the computation of the radial derivatives $\bar{\dot{r}}$. We retained point S_3 as the center for computing them. The mean radial derivatives in the plane projections are $\bar{\dot{r}}_{xy} = 108$, $\bar{\dot{r}}_{xz} = 551$, and $\bar{\dot{r}}_{yz} = 502$. The smallest one is clearly $\bar{\dot{r}}_{xy}$, which thus indicates that the x-y plane is nearly parallel to the main rotation [confirmed by Fig. 10(a)]. Variable z should be therefore avoided for synchronizing Rössler-Ortoleva systems.

This is in agreement with the master stability functions (Fig. 11) since variable z offers a class III synchronization, contrary to variable x and variable y which offer class I and class II synchronization, respectively. We therefore correctly discarded the worst variable (variable z). According to the master stability function, variable x should be preferred for synchronizing Rössler-Ortoleva systems.

IV. SYNCHRONIZABILITY VERSUS OBSERVABILITY

The symbolic observability coefficients were computed according to the procedure developed in Refs. [30,53] and reported in Table I with the mean radial derivative. The variable discarded for each system, either according to the analytical procedure and/or the numerical one, is also provided. First, there is a perfect agreement between the analytical and the numerical procedures, with the exception of the Hindmarsh-Rose system for which the variability in the oscillations is poorly seen in the x-z plane due to the tiny range in which evolve variable z. Second, in most of the cases, the variable providing the greatest observability must be discarded for synchronizing systems. This feature completes our result: A good synchronizability is not necessarily, if not rarely, associated with a full observability. This means that distinguishing different states is very different from determining the phase of the main rotation.

TABLE I. Mean radial derivatives for the five systems here investigated. The values in bold correspond to the main rotation plane when determined using the singular set of 1-regular points. The analytical procedure was not possible for the Rössler-Ortoleva system. Discarded variable and symbolic observability coefficients η_X are also reported.

System	Discarded	$\bar{\dot{r}}$	η_X
Rössler 76		$\bar{\dot{r}}_{yz} = 2.03$	$\eta_{x^3} = 0.88$
		$\bar{\dot{r}}_{xz} = 2.78$	$\eta_{y^3} = 1.00$
	z	$\bar{\dot{r}}_{xy} = \mathbf{1.18}$	$\eta_{z^3} = 0.44$
Lorenz 84	x	$\bar{\dot{r}}_{yz} = \mathbf{0.88}$	$\eta_{x^3} = 0.78$
		$\bar{\dot{r}}_{xz} = 1.08$	$\eta_{y^3} = 0.36$
		$\bar{\dot{r}}_{xy} = 1.05$	$\eta_{z^3} = 0.36$
Lorenz 63	x	$\bar{\dot{r}}_{yz} = \mathbf{20.2}$	$\eta_{x^3} = 0.78$
		$\bar{\dot{r}}_{xz} = 42.4$	$\eta_{y^3} = 0.36$
		$\bar{\dot{r}}_{xy} = 34.7$	$\eta_{z^3} = 0.36$
Hindmarsh-Rose		$\bar{\dot{r}}_{yz} = 0.25$	$\eta_{x^3} = 0.25$
		$\bar{\dot{r}}_{xz} = 0.11$	$\eta_{y^3} = 0.56$
	z	$\bar{\dot{r}}_{xy} = \mathbf{0.25}$	$\eta_{z^3} = 1.00$
Rössler-Ortoleva		$\bar{\dot{r}}_{yz} = 502$	$\eta_{x^3} = 0.36$
		$\bar{\dot{r}}_{xz} = 551$	$\eta_{y^3} = 0.46$
	z	$\bar{\dot{r}}_{xy} = \mathbf{108}$	$\eta_{z^3} = 0.56$

V. CONCLUSION

It is still an open question to determine what were the main ingredients for synchronizability. We here checked that the variables spanning the main rotation of the attractor were the best to use for getting a full synchronization. For three-dimensional systems, we proposed here two possible procedures for discarding the variable which does not provide easily a full synchronization between (nearly) identical systems. The first procedure is purely analytical and is based on the concept of singular sets of 1-regular points whose transverse stability is associated with complex conjugated eigenvalues when they are driving the main rotation of the flow. The corresponding plane is thus spanned by the variables having information about the phase of the dynamics. The relevant role of the sets of 1-regular points in the structure of attractors is also here confirmed; they appear as a very useful and complementary concept to singular points.

For the 5 three-dimenisonal systems we investigated, we correctly discarded the worst variable from the candidate variables for synchronizing systems. For the four algebraically simple three-dimensional systems, this was performed using the analytical approach. The complexity of the fifth system, imposed to use a numerical procedure based on the estimation

of the radial derivative (the derivative along the curvature axis). When the system has a single timescale (when this is not a slow-fast system), the numerical procedure was reliable for discarding the worst variable for synchronizing oscillators. All these results were in agreement with the master stability functions and showed that information about the phase is the key ingredient for synchronizing systems. In the Appendix, we applied our procedures to 2 four-dimensional systems. The numerical approach seems to have strong limitations when there are more than one single rotation or when the main rotation is investigated in a higher-dimensional space. When there are not too many nonlinearities in the governing equations, the analytical approach remains valid. As for three-dimensional systems, too many nonlinear terms prevent successful application. Nevertheless, when it is possible to perform the analysis, we confirmed that the information about the phase associated with the main rotation is the key ingredient indeed.

Observability provided by the coupling variable is in fact a marginal property for assessing the synchronizability of coupled systems. As observed for observability, assessing synchronizability does not depend too much on the dynamics but is rather a structural property mainly depending on the algebraic structure of the governing equations. Rather than the present yes-or-no approach, it would be useful to develop an index in the unit range for assessing synchronizability. This is currently under consideration.

The synchronizability of discrete system is very different in nature and would require a very specific procedure. Typically, a discrete system can be considered as the first-return map to a Poincar section of a continuous flow: The main rotation is therefore removed from the problem. Consequently, a specific approach has to be designed for discrete systems.

ACKNOWLEDGMENTS

I thank Luis A. Aguirre for helpful comments about the draft of this paper and Irene Sendiña Nadal for the computation of the master stability functions.

APPENDIX: TWO FOUR-DIMENSIONAL SYSTEMS

To provide some indications about the potential applicability of our technique to higher-dimensional models, we here investigate two very different four-dimensional systems.

1. The Tang system

Let us start with the Tang system [54]

$$\begin{aligned}\dot{x} &= a(y-x)+yz\\ \dot{y} &= b(x+y)-xz\\ \dot{z} &= cx-dz+yw\\ \dot{w} &= ey-fw+xz,\end{aligned} \tag{A1}$$

which has four nonlinear terms. For the retained parameter values, ths system is not hyperchaotic since its attractor is characterized by a single Lyapunov exponent [55]. This is confirmed by the six plane projections of the attractor (Fig. 12) and the first-return map to a Poincaré section which is a slightly foliated bimodal map (not shown).

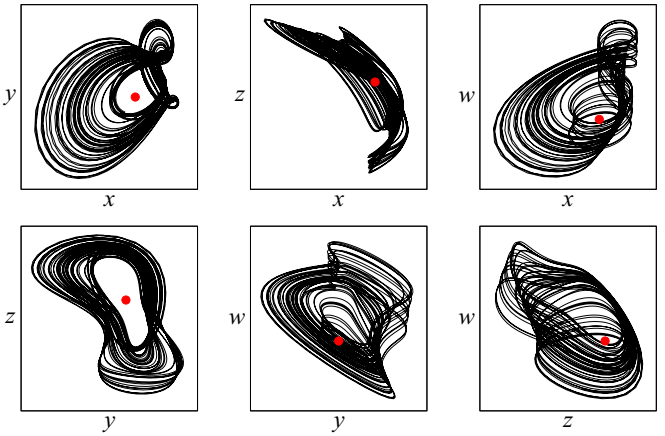

FIG. 12. The six plane projections of the attractor produced by the Tang system (A1). Parameter values: $a = 55$, $b = 25$, $c = 40$, $d = 13$, $e = 23$, and $f = 8$. Initial conditions: $x_0 = 0$, $y_0 = 1$, $z_0 = 0$, and $w_0 = 1$.

This system has two singular points,

$$\mathrm{S}_0 = \begin{vmatrix} x_0 = 0\\ y_0 = 0\\ z_0 = 0\\ w_0 = 0\end{vmatrix} \quad \text{and} \quad \mathrm{S}_* = \begin{vmatrix} x_* = 1.03\\ y_* = 52.77\\ z_* = 1301.53\\ w_* = 319.85\end{vmatrix}. \tag{A2}$$

Point S_* is too far from the attractor to have any influence on its structure. Point S_0 is associated with the eigenvalues

$$\lambda_0 = \begin{vmatrix} 12.30 \pm i\,1316\\ -7.27\\ -13.32\end{vmatrix}; \tag{A3}$$

this is a saddle focus which could govern the main rotation.

We computed the sets of 1-regular points but most of them were too complicated to be correctly investigated. Only the set $\mathcal{S}_z$ leads to eigenvalues with quite simple expression, that is,

$$\Lambda_z = \begin{vmatrix} \frac{b \pm \sqrt{4[ab+(b-a-z)z]+b^2}}{2}\\ -f\end{vmatrix}. \tag{A4}$$

These eigenvalues are not associated with a rotation when $\rho_- < z < \rho_+$ where

$$\rho_\pm = \frac{b-a \pm \sqrt{(a+b)^2+b}}{2}.$$

With the parameter values here retained, this means that this set $\mathcal{S}_z$ is associated with a complex conjugated eigenvalues when $z \notin [56.9; 26.9]$. This set cannot be associated with the main rotation.

We then computed the radial derivatives in each plane projection and got

$$\begin{aligned}\bar{\dot{r}}_{xz} &= 2264 \quad \bar{\dot{r}}_{yw} = 1201\\ \bar{\dot{r}}_{xy} &= 1690 \quad \bar{\dot{r}}_{xw} = 1091\\ \bar{\dot{r}}_{zw} &= 1548 \quad \bar{\dot{r}}_{xy} = 706.\end{aligned}$$

If we consider that the x-z plane projection can clearly not correspond to the main rotation, then the two projections

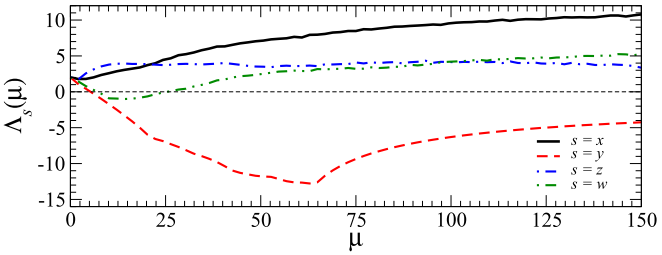

FIG. 13. Master stability functions $\Lambda_s(\mu)$ versus the normalized coupling parameter μ computed for the modified Rössler hyperchaotic systems successively coupled through each of their four variables. Same parameter values as in Fig. 12.

offering the smallest radial derivatives are the plane x-w and x-y (Fig. 12). The x-w plane projection does not provide a clear representation of the main rotation as the y-z projection, for instance. Consequently, the three plane projections for which one of the coordinates is x can be rejected. We therefore quite reliably discard variable x for synchronizing the Tang system.

This is confirmed by the MSF plotted in Fig. 13: Variable x is clearly a variable which cannot allow a full synchronization. We have no argument for rejecting variable z. In fact, a lag synchronization [56] ($\tau = 0.039$ s) is obtained with this variable, which could explain why this variable is not easily discarded. From my point of view this variable has information on the phase but it is delayed. Variable y and w allows full synchronization.

Due to the four nonlinear terms, all variables are providing a poor observability since

$$\eta_{w^4} = \eta_{z^4} = 0.20 > \eta_{x^4} = \eta_{y^4} = 0.15.$$

Such poor observability does not prevent a robust synchronization through variable y.

2. The modified Rössler hyperchaotic system

The second four-dimensional system is the modified Rössler hyperchaotic system [57]

$$\begin{aligned}\dot{x} &= -y - z\\ \dot{y} &= x + (a-1)y + w\\ \dot{z} &= b + xz\\ \dot{w} &= x + (a-d-1)y - cz + (d+1)w\,,\end{aligned} \tag{A5}$$

which produces a hyperchaotic attractor (Fig. 14). For the retained parameter values, the system has two singular points,

$$\mathrm{S}_\pm = \begin{vmatrix} x_\pm = \pm 5.408\\ y_\pm = \pm 0.555\\ z_\pm = \mp 0.555\\ w_\pm = \mp 4.992\end{vmatrix}. \tag{A6}$$

Only the point S_- is surrounded by the attractor. More or less as for the three-dimensional Rössler system [38], the point S_- is responsible for the divergent spiral, and the point S_+ is

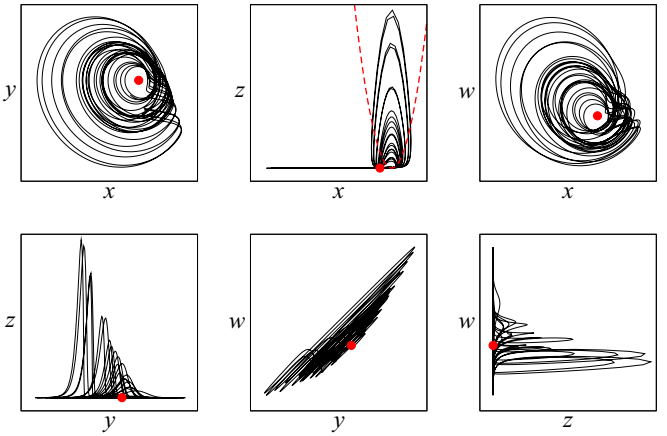

FIG. 14. The six plane projections of the hyperchaotic attractor produced by the modified Rössler hyperchaotic system (A5). Parameter values: $a = 0.25$, $b = 3$, $c = 0.5$, and $d = 0.05$. Initial conditions: $x_0 = -10$, $y_0 = -6$, $z_0 = 0$, and $w_0 = 10.1$.

associated with the nonlinear switch. Their eigenvalues are

$$\lambda_- = \begin{vmatrix} 0.056 \pm i\,1.00\\ 0.097\\ -5.573\end{vmatrix} \quad \text{and} \quad \lambda_+ = \begin{vmatrix} 0.043 \pm i\,0.97\\ 5.268\\ 0.109\end{vmatrix},$$

respectively. Point S_- is a saddle-focus point and point S_+ is an unstable node-focus point.

The set of 1-regular points are quite complicated but their eigenvalues can be often extracted. The set $\mathcal{S}_x$ has real eigenvalues (d, x, a) which cannot be associated with a rotation. Set $\mathcal{S}_y$ is associated with the eigenvalues

$$\lambda_y = \begin{vmatrix} \frac{x \pm \sqrt{x^2 - 4z}}{2}\\ d+1\end{vmatrix}.$$

The first two can be complex conjugated when $z > \frac{x^2}{4}$: As shown in Fig. 14 (x-z plane projection), this corresponds to the domain where the nonlinear switch is active. These complex conjugated eigenvalues are thus associated with the secondary rotation [left part of the attractor shown in the x-z plane projection. The set $\mathcal{S}_z$ of 1-regular points has for eigenvalues

$$\lambda_z = \begin{vmatrix} \frac{a \pm \sqrt{a^2 - 4}}{2}\\ d\end{vmatrix},$$

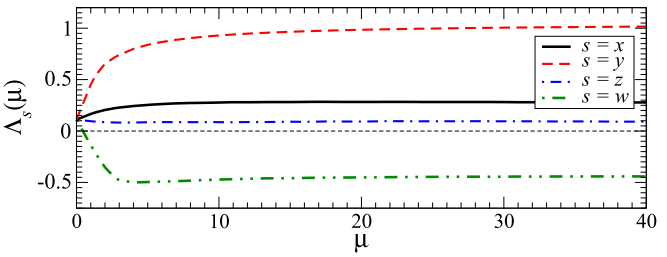

FIG. 15. Master stability functions $\Lambda_s(\mu)$ versus the normalized coupling parameter μ computed for the modified Rössler hyperchaotic systems successively coupled through each of their four variables. Same parameter values as in Fig. 14.

which are always complex conjugated for the retained parameter values. This set is clearly associated with the main rotation. The set $\mathcal{S}_w$ is too complicated to be treated. The probability for having complex conjugated eigenvalues over the whole state is very low. This analysis therefore leads to associate set $\mathcal{S}_z$ with the main rotation and to discard variable z for synchronizing them. The present theory cannot do better than discarding the worst variable. Radial derivatives, computed in the six plane projections, do not provide useful information; they are even misleading.

Using the MSF shown in Fig. 15, variable z cannot allow synchronizatin of two copies of this hyperchaotic system. For now, there is no agreement to discard variables x and y which cannot provide neither full synchronization nor any other type of synchronization. As for the Rössler systems, there is a relationship between synchronizability and observability since

$$\eta_{x^4} = \eta_{y^4} = 0.79 > \eta_{w^4} = 0.50 > \eta_{z^4} = 0.44\,,$$

that is, the variable offering the poorest observability does not allow us to synchronize two hyperchaotic systems (A5).

[1] J. H. Vincent, On some experiments in which two neighboring maintained oscillatory circuits affect a resonating circuit, Proc. Phys. Soc. Lond. **32**, 84 (1919).

[2] E. V. Appleton, The automatic synchronization of triode oscillators, Proc. Cambr. Philos. Soc. **21**, 231 (1922).

[3] H. S. Möller, Uber störungsfreien Gleichstromempfang mit den Schwingaudion, Taschenb. drahtlos. Telegr. Telephon. **17**, 256 (1921).

[4] J. Mercier, Sur la synchronisation harmonique des oscillateurs électriques, Compt. Rend. Acad. Sci. **174**, 448 (1922).

[5] J. Mercier, De la synchronisation harmonique et multiple, J. Phys. Rad. **5**, 168 (1924).

[6] D. G. Tucker, Forced oscillations in oscillator circuits, and the synchronization of oscillators, J. Inst. Electr. Eng. **93**, 57 (1945).

[7] C. Hayashi, *Noninear Oscillations in Physical Aystems* (McGraw–Hill, New York, 1964).

[8] E. E. David, Some aspects of r-f phase control in microwave oscillators, Research Laboratory of Electronics (MIT), Technical Report No. 100 (1949).

[9] L. M. Pecora and T. L. Carroll, Synchronization in Chaotic Systems, Phys. Rev. Lett. **64**, 821 (1990).

[10] S. Boccaletti, J. Kurths, G. Osipov, D. L. Valladares, and C. S. Zhou, The synchronization of chaotic systems, Phys. Rep. **366**, 1 (2002).

[11] A. Pikovsky, M. Rosenblum, and J. Kurths, *Synchronization: A Universal Concept in Nonlinear Sciences* (Cambridge University Press, Cambridge, 2003).

[12] M. Chavez, D.-U. Hwang, A. Amann, H. G. E. Hentschel, and S. Boccaletti, Synchronization is Enhanced in Weighted Complex Networks, Phys. Rev. Lett. **94**, 218701 (2005).

[13] I. Sendiña-Nadal, I. Leyva, A. Navas, J. A. Villacorta-Atienza, J. A. Almendral, Z. Wang, and S. Boccaletti, Effects of degree correlations on the explosive synchronization of scale-free networks, Phys. Rev. E **91**, 032811 (2015).

[14] A. A. King, W. M. Schaffer, C. Gordon, J. Treat, and M. Kot, Weakly dissipative predator-prey systems, Bull. Math. Biol. **58**, 835 (1996).

[15] P. Glendinning, Inaccessible attractors of weakly dissipative systems, Nonlinearity **10**, 507 (1997).

[16] A. Celletti, Weakly dissipative systems in celestial mechanics, Lect. Notes Phys. **729**, 67 (2007).

[17] D. S. A. Júnior, M. L. Santos, and J. E. Muñoz Rivera, Stability to weakly dissipative timoshenko systems, Math. Methods Appl. Sci. **36**, 1965 (2012).

[18] L. M. Pecora and T. L. Carroll, Master Stability Functions for Synchronized Coupled Systems, Phys. Rev. Lett. **80**, 2109 (1998).

[19] S. Boccaletti, V. Latora, Y. Moreno, M. Chavez, and D.-U. Hwang, Complex networks: Structure and dynamics, Phys. Rep. **424**, 175 (2006).

[20] T. Stojanovski, L. Kocarev, and R. Harris, Applications of symbolic dynamics in chaos synchronization, IEEE Trans. Circ. Syst. I **44**, 1014 (1997).

[21] S. D. Pethel, N. J. Corron, Q. R. Underwood, and K. Myneni, Information Flow in Chaos Synchronization: Fundamental Tradeoffs in Precision, Delay, and Anticipation, Phys. Rev. Lett. **90**, 254101 (2003).

[22] L. Freitas, L. A. B. Torres, and L. A. Aguirre, Phase definition to assess synchronization quality of nonlinear oscillators, Phys. Rev. E **97**, 052202 (2018).

[23] C. Letellier and L. A. Aguirre, On the interplay among synchronization, observability and dynamics, Phys. Rev. E **82**, 016204 (2010).

[24] I. Sendiña-Nadal, S. Boccaletti, and C. Letellier, Observability coefficients for predicting the class of synchronizability from the algebraic structure of the local oscillators, Phys. Rev. E **94**, 042205 (2016).

[25] L. A. Aguirre and C. Letellier, Controllability and synchronizability: Are they related? Chaos Soliton. Fract. **83**, 242 (2016).

[26] G. V. Osipov, B. Hu, C. Zhou, M. V. Ivanchenko, and J. Kurths, Three Types of Transitions to Phase Synchronization in Coupled Chaotic Oscillators, Phys. Rev. Lett. **91**, 024101 (2003).

[27] M. C. Romano, M. Thiel, J. Kurths, I. Z. Kiss, and J. L. Hudson, Detection of synchronization for non-phase-coherent and non-stationary data, Europhys. Lett. **71**, 466 (2005).

[28] I. Z. Kiss, Q. Lv, and J. L. Hudson, Synchronization of non-phase-coherent chaotic electrochemical oscillations, Phys. Rev. E **71**, 035201(R) (2005).

[29] C. Letellier and L. A. Aguirre, Symbolic observability coefficients for univariate and multivariate analysis, Phys. Rev. E **79**, 066210 (2009).

[30] E. Bianco-Martinez, M. S. Baptista, and C. Letellier, Symbolic computations of nonlinear observability, Phys. Rev. E **91**, 062912 (2015).

[31] C. Letellier and J.-M. Malasoma, Architecture of chaotic attractors for flows in the absence of any singular point, Chaos **26**, 063115 (2016).

[32] O. E. Rössler, Chaotic behavior in simple reaction system, Z. Naturforsch., A **31**, 259 (1976).
[33] P. Glendenning and C. Sparrow, Local and global behavior near homoclinic orbit, J. Stat. Phys. **35**, 645 (1984).
[34] A. Arnéodo, F. Argoul, J. Elezgaray, and P. Richetti, Homoclinic chaos in chemical systems, Physica D **62**, 134 (1993).
[35] C. Letellier, J. Maquet, H. Labro, L. L. Sceller, G. Gouesbet, F. Argoul, and A. Arnéodo, Analyzing chaotic behavior in a Belousov-Zhabotinskii reaction by using a global vector field reconstruction, J. Phys. Chem. A **102**, 10265 (1998).
[36] C. Letellier and L. A. Aguirre, Required criteria for recognizing new types of chaos: Application to the "cord" attractor, Phys. Rev. E **85**, 036204 (2012).
[37] L. A. Aguirre, L. L. Portes, and C. Letellier, Observability and synchronization of neuron models, Chaos **27**, 103103 (2017).
[38] C. Letellier, P. Dutertre, and B. Maheu, Unstable periodic orbits and templates of the Rössler system: Toward a systematic topological characterization, Chaos **5**, 271 (1995).
[39] C. Letellier, L. A. Aguirre, and J. Maquet, Relation between observability and differential embeddings for nonlinear dynamics, Phys. Rev. E **71**, 066213 (2005).
[40] R. Hermann and A. Krener, Nonlinear controllability and observability, IEEE Trans. Autom. Contr. **22**, 728 (1977).
[41] C. Letellier, J. Maquet, L. L. Sceller, G. Gouesbet, and L. A. Aguirre, On the non-equivalence of observables in phase-space reconstructions from recorded time series, J. Phys. A **31**, 7913 (1998).
[42] M. Frunzete, J.-P. Barbot, and C. Letellier, Influence of the singular manifold of nonobservable states in reconstructing chaotic attractors, Phys. Rev. E **86**, 026205 (2012).
[43] O. E. Rössler, An equation for continuous chaos, Phys. Lett. A **57**, 397 (1976).
[44] E. N. Lorenz, Irregularity: A fundamental property of the atmosphere, Tellus A **36**, 98 (1984).
[45] I. Sendiña-Nadal and C. Letellier, Synchronizability of nonidentical weakly dissipative systems, Chaos **27**, 103118 (2017).
[46] E. N. Lorenz, Deterministic nonperiodic flow, J. Atmos. Sci. **20**, 130 (1963).
[47] C. Letellier and R. Gilmore, Covering dynamical systems: Twofold covers, Phys. Rev. E **63**, 016206 (2000).
[48] A. L. Hodgkin and A. F. Huxley, A quantitative description of membrane current and its application to conduction and excitation in nerve, J. Physiol. **117**, 500 (1952).
[49] R. FitzHugh, Impulses and physiological states in theoretical models of nerve membrane, Biophys. J. **1**, 445 (1961).
[50] J. L. Hindmarsh and R. M. Rose, A model of neuronal bursting using three coupled first order differential equations, Proc. R. Soc. Lond. B **221**, 87 (1984).
[51] O. E. Rössler and P. J. Ortoleva, Strange attractors in 3-variable reaction systems, Lect. Notes Biomath. **21**, 67 (1978).
[52] G. Byrne, R. Gilmore, and C. Letellier, Distinguishing between folding and tearing mechanisms in strange attractors, Phys. Rev. E **70**, 056214 (2004).
[53] C. Letellier, I. Sendiña-Nadal, E. Bianco-Martinez, and M. S. Baptista, A symbolic network-based nonlinear theory for dynamical systems observability, Sci. Rep. **8**, 3785 (2018).
[54] L. Tang, L. Zhao, and Q. Zhang, *A Novel Four-dimensional Hyperchaotic System* (Springer-Verlag, Berlin, 2011), pp. 392–401.
[55] J. P. Singh and B. Roy, The nature of Lyapunov exponents is $(+, +, -, -)$. Is it a hyperchaotic system? Chaos Soliton. Fract. **92**, 73 (2016).
[56] M. G. Rosenblum, A. S. Pikovsky, and J. Kurths, From Phase to Lag Synchronization in Coupled Chaotic Oscillators, Phys. Rev. Lett. **78**, 4193 (1997).
[57] A. Tamasevicius and A. Cenys, Synchronizing hyperchaos with a single variable, Phys. Rev. E **55**, 297 (1997).